Chinese Chemical Letters 35 (2024) 109357

Contents lists available at ScienceDirect

Chinese Chemical Letters

journal homepage: www.elsevier.com/locate/cclet

Vapor-phase postsynthetic amination of hypercrosslinked polymers for efficient iodine capture

Pengcheng Su[a,b,1], Shizheng Chen[b,1], Zhihong Yang[c,*], Ningning Zhong[a], Chenzi Jiang[a], Wanbin Li[b,*]

[a] School of Materials and Chemical Engineering, Anhui Jianzhu University, Hefei 230026, China
[b] School of Environment, Jinan University, Guangzhou 511443, China
[c] Jiangsu Environmental Protection Group Nantong Co., Ltd., Nantong 226010, China

ARTICLE INFO

Article history:
Received 13 September 2023
Revised 12 November 2023
Accepted 1 December 2023
Available online 3 December 2023

Keywords:
Porous polymers
Postsynthetic amination
Hypercrosslinked polymers
Vapor-phase grafting
Iodine capture

ABSTRACT

Hypercrosslinked polymers (HCPs) with large surface areas, high intrinsic porosities and low production costs may be available platforms for iodine capture. However, the lack of iodine-philicity binding sites limits their adsorption capacity. Here we use vapor-phase postsynthetic amination strategy to introduce electron-donating amino groups into the prefabricated HCPs for enhancing their iodine capture performance. Through simple vapor-phase exposure, the halogen-containing HCPs can be grafted by amines through nucleophilic substitution toward chloro groups. Combining with the abundant amino groups and high porosities, the amino-functionalized porous polymers show substantially increased iodine adsorption capacity, about 221% as that of original one, accompanied by excellent recyclability. Mechanism investigations reveal the key roles of the electron-donor amino groups and π-conjugated benzene rings along with structure characteristics of porous polymer frameworks in iodine capture. Moreover, this vapor-phase amination strategy shows good generality and can be extended to various amines, *e.g.*, ethylenediamine, 1,3-diaminopropane and diethylenetriamine. Our work proves that this simple vapor-phase postsynthetic functionalization strategy may be applied in other porous polymers with wide application prospects in adsorption, separation and storage.

Nuclear power makes great contribution to the world's energy supply and sustainable development, owing to ultrahigh energy density and low carbon emission [1,2]. However, the volatile radioactive wastes from spent nuclear fuels such as radioactive iodine cause enormous safety issues, since it has an extremely long radioactive half-life and significant risk to ecological environment and human health [3]. In contrast with traditional liquid scrubbing method, adsorption possesses many unique features such as high capture efficiency and capacity, easy operation and low cost [4]. Crystalline porous materials, *e.g.*, metal–organic frameworks (MOFs) and covalent organic frameworks (COFs), displayed excellent iodine capture performances, but the relatively high production costs hinder their wide applications [5,6]. As a subclass of porous organic polymers, hypercrosslinked polymers (HCPs) are synthesized from the high degree crosslinking polymerization of aromatic monomer based on Friedel–Crafts chemistry [7–11]. The extensive and strong crosslinking of polymer chains endow HCPs with large surface area, permanent porosity, diverse structures and excellent stability. Although a great diversity of aromatic monomers gives rise to the abundance of HCPs with various pore architectures, the lack of electron-donor binding sites limits their iodine adsorption capacity.

Adsorption performances of porous polymers are decided by their textural properties (*e.g.*, surface area and pore size) and functional components. Porous polymers with accessible channels and abundant electron-donating moieties/groups will particularly show high adsorption capacity toward iodine molecules [12,13]. Recently, the functional porous polymers are synthesized mainly through ingenious predesign and postsynthetic functionalization [14,15]. For the predesign, the monomers with functional groups or molecules are used as building blocks and further polymerized or assembled into porous polymers with desired functionality. There are several predesign strategies to improve the adsorption of porous polymers for iodine species through forming charge-transfer interactions: (1) introducing the electron-rich N sites (*e.g.*, imine and triazine moieties) [16–19]; (2) constructing π-conjugated structures (*e.g.*, ben-

* Corresponding authors.
E-mail addresses: yangzhjsep@163.com (Z. Yang), gandeylin@126.com (W. Li).
[1] These authors contributed equally to this work.

https://doi.org/10.1016/j.cclet.2023.109357
1001-8417/

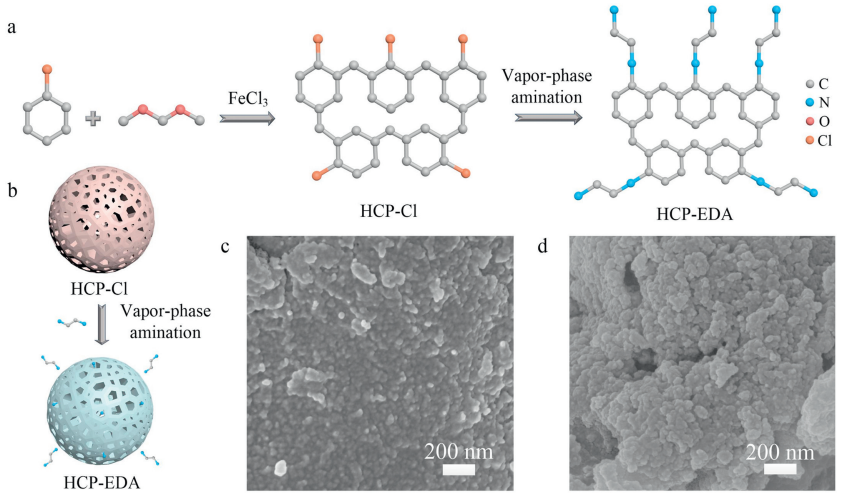

Fig. 1. Vapor-phase amination of HCPs. (a) Synthesis of HCP-Cl through Friedel-Crafts reaction of chlorobenzene with FDA cross-linker and subsequent vapor-phase postsynthetic amination. (b) Schematic illustration of vapor-phase amination of HCP-Cl to HCP-EDA. SEM images of (c) HCP-Cl and (d) HCP-EDA particles.

zene rings) [20,21]; (3) doping with nucleophilic heteroatoms (*e.g.*, sulfur, phosphorus and boron) [22,23]. Although porous polymers synthesized by predesign solvothermal reaction have obtained great progresses, the introduced functional segments may disturb the efficient polymerization of monomers and thus lead to the failure for synthesizing some specific materials [24–26]. Postsynthetic functionalization usually refers to introduce the functional groups/molecules into the parent porous polymers for obtaining anticipated functionalities [27–29]. For example, incorporation of ionic liquid (2-bromoethyl)trimethylammonium bromide into COFs could promote the adsorption of iodine molecules *via* strong Coulomb interactions [30]. In terms of synthesis and modification processes, most of these porous polymers are implemented in rigorous liquid-based medium, still facing many issues, *e.g.*, the difficulty in controlling reaction processes, the reagent solubility and vast consumption of organic solvents [31–33].

Vapor-phase processing (VPP), based on the vapor-phase reaction of vaporized substances, has been applied in chemical vapor deposition and functionalization of polymers, inorganics and crystalline porous materials, thanks to its excellent controllability, high reactivity, environmental friendliness, *etc.* [34–37]. For example, *p*-phenylenediamine vapor could react with 1,3,5-triformylphloroglucinol through solid–vapor interfacial polymerization to deposit COFs [38]. Besides chemical deposition, VPP can also be utilized for postsynthetic functionalization of porous materials to tune their physicochemical properties [39]. In our recent works, we have used vapor-phase linker exchange and grafting to tune the pore channels and adsorption behaviors of MOFs [40–42]. Up to now, there is few report about the vapor-phase modification of HCPs. Considering the large surface areas, high porosities and abundant modifiable sites of HCPs, we envisage whether vapor-phase processing can be applied to modify parent HCPs for enhancing their iodine adsorption performances. Herein, we report a simple vapor-phase postsynthetic amination strategy to graft electron-rich amino groups into the halogen-containing HCPs through nucleophilic substitution of amines toward chloro groups (Figs. 1a and b). The introduced amino groups can act as active electron-donating binding sites to enhance the iodine capture performances of HCPs.

As a common aromatic monomer, chlorobenzene was used to fabricate halogen-containing HCP-Cl as probe for iodine capture, owing to the high reactivity, low cost and abundant modifiable sites. In this study, the brown HCP-Cl powders could be obtained through a simple one-step Friedel-Crafts reaction using formaldehyde dimethyl acetal (FDA) as an external cross-linker (Figs. S1 and S2 in Supporting information) [7,43,44]. Scanning electron microscopy (SEM) image of HCP-Cl (Fig. 1c) indicated the formation of spherical particles with size smaller than 50 nm, which was in consistent with the previous literature [7]. After successful preparation, the HCP-Cl powders were exposed to ethylenediamine (EDA) vapor with different times for preparation of amino functionalized HCP-EDA$_x$, where x represented the amination times of 0.2, 1, 3 and 12 h. Under the thermal treatment of 393 K, the vaporized ethylenediamine molecules diffused into the surfaces and pores of the prefabricated HCP-Cl particles and then triggered the nucleophilic substitution of amines toward chloro groups through the vapor–solid reactions (Figs. S3 and S4 in Supporting information). The aminated HCP-EDA became darker with the extension of amination time and showed similar particle morphology with HCP-Cl (Fig. 1d and Fig. S2). As shown in Fourier transformation infrared (FTIR) spectra of HCP-EDA, the characteristic peaks of N–H bond at 671 and 3426 cm^{-1} increased significantly, while the C–Cl peak at 818 cm^{-1} attenuated (Fig. 2a and Fig. S5 in Supporting information). These FTIR peak variations proved the successful grafting of ethylenediamine into HCP-EDA. The peak at 3456 cm^{-1} for HCP-Cl may originate from the residual hydroxymethyl alkanes, which were produced by the secondary reaction of vastly used FDA cross-linker during the polymerization [24,45]. The appearance of benzene ring peak in HCP-EDA demonstrated the well maintenance of polymer frameworks.

X-ray photoelectron spectra (XPS) characterization of HCP powders was conducted to investigate the elemental binding states and contents. Relative to HCP-Cl with C–C/C=C and C–Cl peaks in the high-resolution C 1s XPS profile, a new C–N peak from ethylenediamine emerged at 285.8 eV for HCP-EDA and the peak intensity gradually raised with the increase of amination time, while the peak intensity of C–Cl decreased (Fig. 2b and Fig. S6 in Supporting information). The contents of C–N and C–Cl bonds in HCP-EDA were quantitatively analyzed according to their integral areas of C 1s XPS peaks. The C–N peak area expanded from 0% for HCP-Cl to 4.56% for HCP-EDA$_{12}$, while C–Cl peak declined from 9.48% to 5.76% (Table S1 in Supporting information). Moreover, in the N 1s spectra of HCP-EDA, two new C–N and N–H bonds appeared at 399.1 and 400.8 eV, respectively (Fig. 2c). The longer amination time led to stronger C–N and N–H peaks along with the gradually increased N contents in HCP-EDA (Fig. S7 and Table S2 in Supporting information), similar to the FTIR results. For example, the N content of HCP-EDA$_3$ reached at 5.33%, while HCP-Cl showed no

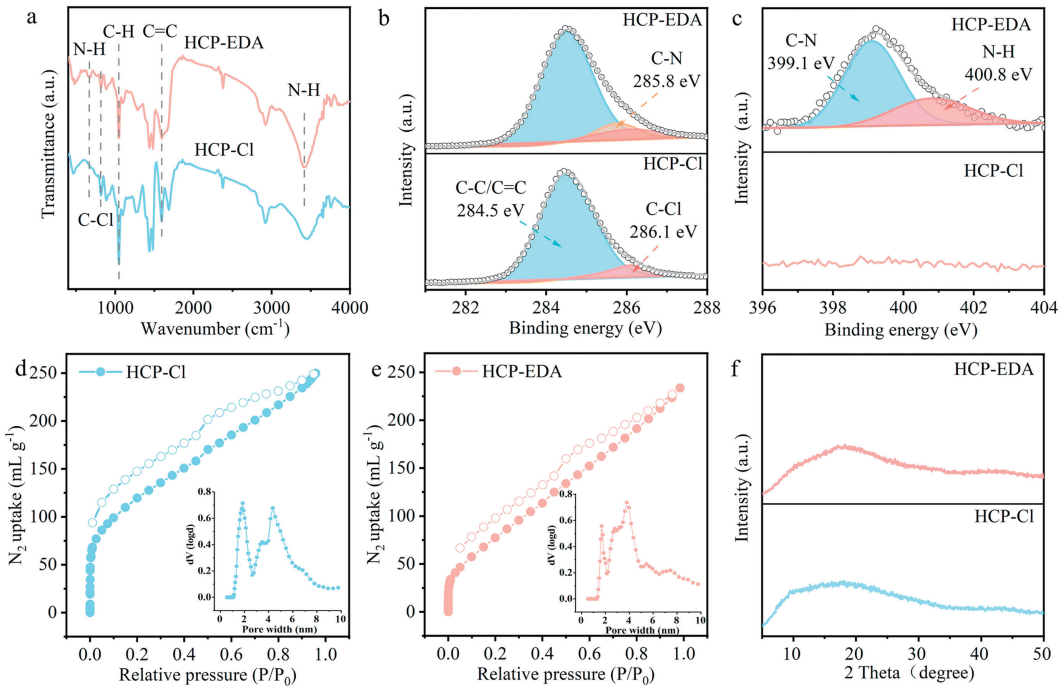

Fig. 2. Characterizations of HCP-Cl and HCP-EDA with amination time of 3 h. (a) FTIR spectra of HCP-Cl and HCP-EDA. (b) C 1s XPS spectra of HCP-Cl and HCP-EDA. (c) N 1s XPS spectra of HCP-Cl and HCP-EDA. N_2 adsorption–desorption isotherms of (d) HCP-Cl and (e) HCP-EDA. The insets are pore width distribution patterns calculated by DFT model. (f) XRD patterns of HCP-Cl and HCP-EDA.

detected N element. It should be noted that the N content only showed slight fluctuation with the extension of amination time to 12 h. This might be interpreted by the fact that vapor-phase exposure with 3 h was sufficient to allow the nucleophilic substitution reaction to reach equilibrium or realize maximum. All these characterizations proved the successful grafting of ethylenediamine into HCP-EDA through vapor-phase amination.

Nitrogen adsorption-desorption isotherms were measured at 77 K to investigate the porous properties of HCP-Cl and HCP-EDA (Figs. 2d, e and Fig. S8 in Supporting information). The Brunauer–Emmett–Teller (BET) specific surface area and pore volume of HCP-Cl were 431 m^2/g and 0.39 mL/g, respectively. Due to the incorporation of ethylenediamine molecules, the surface areas and pore volumes of the HCP-EDA particles decreased (Table S3 in Supporting information). For example, the BET surface area and pore volume of HCP-EDA_{12} were 291 m^2/g and 0.32 mL/g, respectively. As shown in the Fig. 2e, a rapid N_2 uptake emerged at relatively low pressure ($P/P_0 < 0.01$) and a hysteresis loop appeared during the desorption process in HCP-EDA isotherm, proving the existence of abundant micropore and mesopore structures, respectively. The formation of hierarchical pores may originate from the highly crosslinking polymerization of adjacent benzene rings through -CH_2- bridges [46,47]. Moreover, the pore width distributions calculated by nonlocal density functional theory (NLDFT) revealed the dual-pore structure of HCP-Cl with the sizes of 1.9 and 4.3 nm, respectively (Fig. 2d). Owing to the grafting of ethylenediamine molecules, the pore sizes of HCP-EDA reduced (Fig. 2e and Fig. S8 in Supporting information). The prepared HCPs had also been characterized by X-ray diffraction (XRD). Clearly, like most of amorphous polymers, the XRD patterns of HCP-Cl and HCP-EDA particles displayed a characteristic broad peak, revealing that they were amorphous in nature (Fig. 2f). The above analyses validate that HCP-EDA has abundant electron-donating amino groups, large surface areas and hierarchical pore structures, which may be beneficial for iodine capture.

The capture of radioiodine has received increasing interests due to the potential treatment of nuclear wastes [48–50]. In this study, HCP-EDA particles with well-defined porous structures as well as abundant electron-donating amino groups were employed in iodine vapor capture at 348 K. As shown in Fig. 3a, the iodine uptakes of HCP-Cl and HCP-EDA sharply increased with the longer adsorption time and then reached at adsorption equilibrium after about 30 h. In contrast with HCP-Cl, the HCP-EDA powders showed significantly improved iodine capture amounts owing to the introduction of electron-donating amino adsorption sites. For example, HCP-EDA_3 displayed the iodine uptake of 1977 mg/g, about 221% as that of HCP-Cl (895 mg/g), revealing its superiority in iodine capture. Obviously, such a high iodine adsorption capacity of HCP-EDA surpassed most reported absorbents including inorganic particles, metal-organic frameworks and porous organic polymers (Table S7 in Supporting information). It was worth noting that HCP-EDA_{12} displayed similar adsorption capacity in contrast with HCP-EDA_3 since they possessed analogous N contents and surface areas.

To study the iodine adsorption kinetics of HCPs, the typical *pseudo*-second-order kinetic model was adopted to fit the experimental adsorption data as a function of adsorption time (Fig. 3b). The values of the calculated correlation coefficients (R^2) and kinetic constants (k_2) were illustrated in Table S4 (Supporting information). Results suggested that the iodine adsorption processes of HCP-EDA fitted well in pseudo-second-order kinetic model on the basis of high correlation coefficients [51,52]. It confirmed that the high adsorption amounts mainly came from the strong chemical interactions between the electron donor–acceptor pairs of amino groups and iodine molecules. To further evaluate the adsorption rates, we calculated the rate constants using the adsorption capacity and equilibrium time. The rate constant of HCP-EDA ($66\ mg\ g^{-1}\ h^{-1}$) was similar with those of other adsorbents (Table S7 in Supporting information). $K_{80\%}$ parameter was also calculated through dividing 80% saturated adsorption amount by corresponding adsorption time [6,23]. Fig. S9 (Supporting information) indicated the relationship between saturated adsorption capacity and $K_{80\%}$ value of various adsorbents. The adsorption performance of the HCP-EDA could surpass the original HCP-Cl and

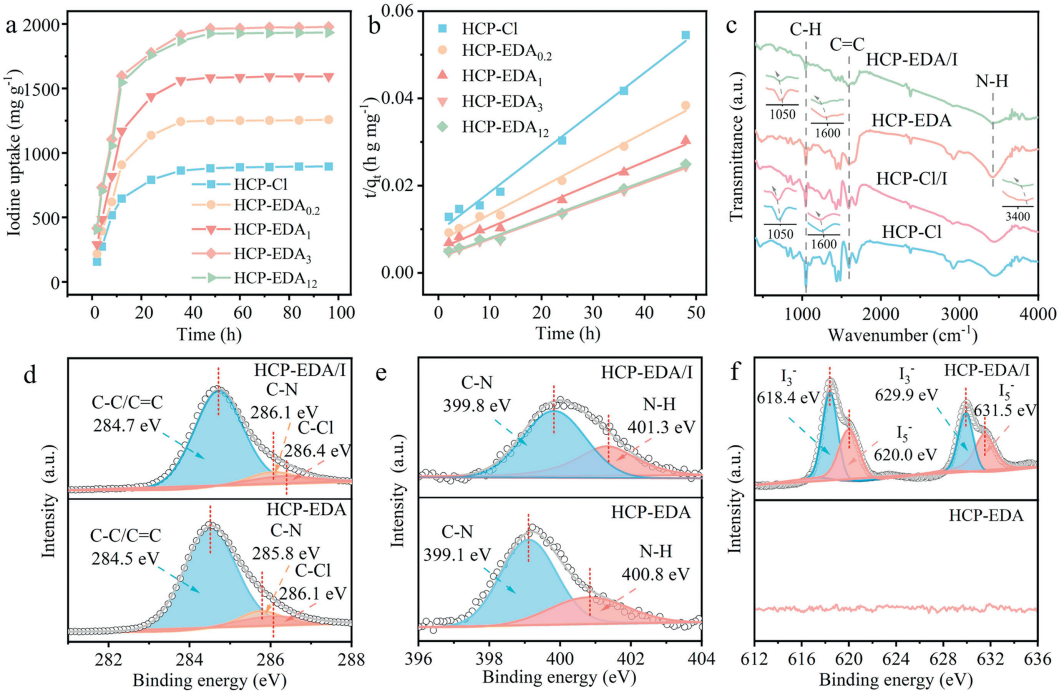

Fig. 3. Iodine adsorption behavior and mechanism. (a) Time-dependent iodine adsorption by HCP-Cl and HCP-EDA at 348 K in saturated iodine vapor. (b) Plots of *pseudo*-second-order adsorption kinetics fitting for iodine over HCP-Cl and HCP-EDA. (c) FTIR spectra of HCP-Cl and HCP-EDA with the amination time of 3 h before and after iodine adsorption. (d) C 1s XPS spectra of HCP-EDA and HCP-EDA/I. (e) N 1s XPS spectra of HCP-EDA and HCP-EDA/I. (f) I 3d XPS spectra of HCP-EDA and HCP-EDA/I.

most reported adsorbents. Although COFs showed high adsorption capacities, their expensive monomers usually resulted in high production costs and thus restricted the practical application [3]. Furthermore, we conducted the reusability test of HCP-EDA by heating the iodine adsorbed powders at 393 K. After five adsorption-regeneration cycles, the adsorption capacity of HCP-EDA powders only displayed slight fluctuations owing to the inherent chemical stability (Fig. S10 in Supporting information). To further investigate the stability and recyclability of HCP-EDA, we conducted the FTIR characterization. The regenerated HCP-EDA showed identical FTIR spectra as original one (Fig. S11 in Supporting information), which proved the well-maintained chemical structures. It should be noted that iodine molecules could desorb from HCP-EDA during the regeneration process, indicating the presence of weak physical bonding interactions. The physical adsorption of iodine in the cavity of the frameworks contributed to improve the adsorption rates. These adsorption behaviors validated that the amino-functionalized HCP-EDA particles could be well used for industrial iodine capture with high adsorption capacity and excellent recyclability.

To understand the iodine adsorption mechanism, FTIR and XPS characterization were implemented on HCP-Cl and HCP-EDA before and after iodine adsorption. As shown in Fig. 3c, the bonds associated with C–H and C=C on the benzene rings after iodine adsorption shifted from 1049 cm^{-1} to 1597 cm^{-1} for HCP-Cl to 1042 and 1589 cm^{-1} for HCP-Cl/I. For HCP-EDA/I, the C–H and C=C bonds displayed similar skewing, while the peak intensities largely attenuated. These peak alterations in positions and intensities proved that the structural benzene moieties in the framework of HCP-EDA acted as adsorption sites for trapping iodine molecules. In addition, the characteristic bond of N–H for HCP-EDA/I shifted from 3426 cm^{-1} to 3410 cm^{-1}, accompanied with the degeneration in peak intensity. Such a deviation in FTIR spectra of HCP-EDA before and after iodine adsorption proved the existence of strong charge-transfer interactions between the electron-rich amino groups and the electron-deficient iodine molecules [25,53].

High resolution XPS spectra of HCP-EDA before and after iodine adsorption were measured to investigate chemical binding states. The peaks of C–C/C=C, C–N and C–Cl bonds in C 1s XPS spectra of HCP-EDA/I shifted from 284.5, 285.8 and 286.1 eV to 284.7, 286.1 and 286.4 eV after iodine adsorption (Fig. 3d). The N 1s XPS spectra also showed that the peaks at 399.1 and 400.8 eV, assigned to C–N and N–H bonds in HCP-EDA, shifted to 399.8 and 401.3 eV for HCP-EDA/I, respectively (Fig. 3e), proving the formation of charge-transfer complexes between iodine and amino groups [2]. As shown in Fig. 3f, I 3d XPS characterization was conducted to analyze the nature of captured iodine. Compared to HCP-EDA, the I 3d spectra of HCP-EDA/I showed the I $3d_{3/2}$ binding energies at 618.4 and 629.9 eV as well as I $3d_{5/2}$ signals at 620.0 and 631.5 eV. The contents of I_3^- and I_5^- were quantitatively calculated through their integral peak areas in XPS spectra. As a result, I_3^- and I_5^- species occupied 52% and 48% of the total iodine uptake content, respectively. The dominant components of I_3^- and I_5^- in HCP-EDA/I validated the charge transfer between iodine and adsorption sites (N–H and benzene) to produce polyiodide anions [2,54].

Owing to the incorporation of ethylenediamine molecules, the pore sizes of HCP-EDA reduced, but still maintaining abundant micropore and mesopore structures. During the iodine adsorption process, the porous polymer frameworks of HCPs contributed to the fast diffusion of iodine molecules (Fig. S12a in Supporting information). Since HCPs possessed multitudinous benzene rings with π-conjugated structures, charge transfer interactions formed between the iodine and benzene rings, leading to the high adsorption amount [55]. Moreover, the grafted electron-rich amino groups could act as strong electron donor binding sites to form charge transfer complexes and enhance iodine capture capacity (Fig. S12b in Supporting information) [56–58]. Based on these insights, we attributed the excellent iodine capture performances of HCP-EDA to the presence of a large number of electron-donating amino groups and benzene rings as iodine-philic binding sites as well as porous structure characteristics.

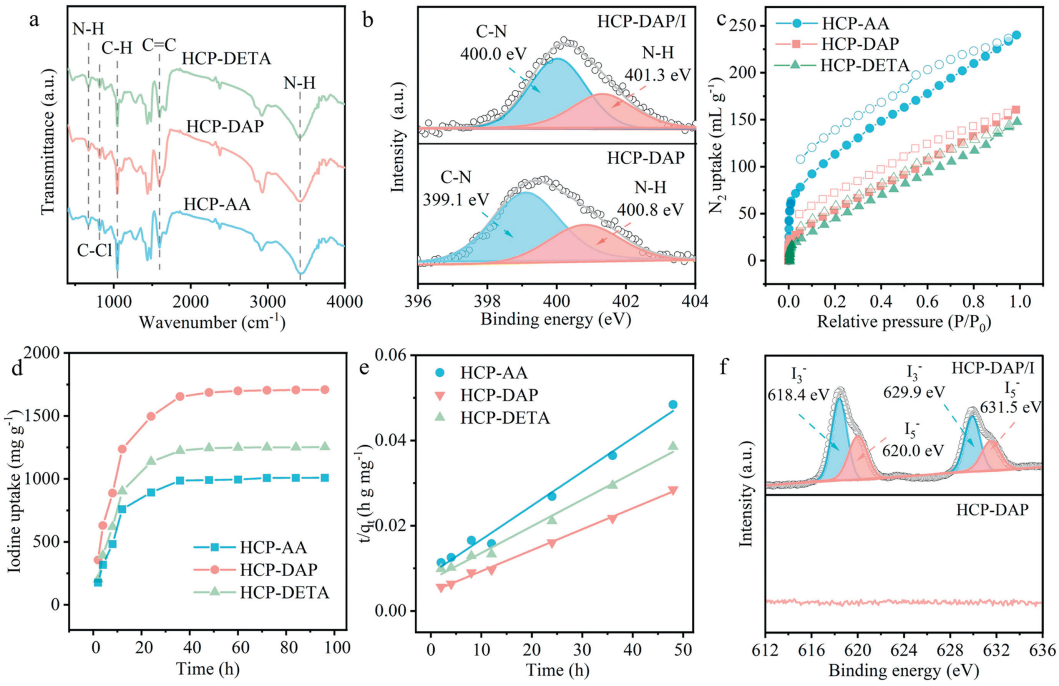

Fig. 4. Generality of vapor-phase amination. (a) FTIR spectra of HCP-AA, HCP-DAP and HCP-DETA. (b) N 1s XPS spectra of HCP-DAP and HCP-DAP/I. (c) Nitrogen adsorption-desorption isotherms of HCP-AA, HCP-DAP and HCP-DETA. (d) Iodine adsorption curves of HCP-AA, HCP-DAP and HCP-DETA at 348 K in saturated iodine vapor. (e) Plots of *pseudo*-second-order adsorption kinetics fitting for iodine over HCP-AA, HCP-DAP and HCP-DETA. (f) I 3d XPS spectra of HCP-DAP and HCP-DAP/I.

To evaluate the generality of vapor-phase amination strategy, various amines including aqueous ammonia (AA), 1,3-diaminopropane (DAP) and diethylenetriamine (DETA) were used to modify HCP-Cl under same condition with the amination time of 3 h (Fig. S13 in Supporting information). Through vapor-phase exposure, the dark brown HCP-AA, HCP-DAP and HCP-DETA powders were obtained (Fig. S14 in Supporting information). SEM images showed that HCP-DAP possessed similar particle morphology with HCP-Cl and HCP-EDA (Fig. S15 in Supporting information). The FTIR spectra of HCP-AA, HCP-DAP and HCP-DETA showed the appearance of N–H peak at 671 and 3426 cm^{-1} as well as the diminution of C–Cl peak at 818 cm^{-1} in contrast with HCP-Cl (Fig. 4a). Like FTIR spectra, XPS characterization showed that a new C–N peak and two new C–N and N–H peaks emerged in C 1s and N 1s spectra of HCP-DAP, respectively (Fig. 4b and Fig. S16 in Supporting information). These results validated that various amines could be applied in vapor-phase amination. Nitrogen adsorption-desorption isotherms were measured to investigate the porous properties of HCPs (Fig. 4c). HCP-AA, HCP-DAP and HCP-DETA exhibited the BET surface areas of 410, 217 and 180 m^2/g, and pore volumes of 0.37, 0.25 and 0.23 mL/g, respectively (Table S5 in Supporting information). In contrast with HCP-AA, the surface areas of HCP-DAP and HCP-DETA largely reduced, owing to the introduction of 1,3-diaminopropane and diethylenetriamine with long molecular chains. Pore size distribution patterns also showed that the peak intensities at pore sizes of 1.9 and 4.3 nm for HCP-DAP and HCP-DETA decreased sharply (Fig. S17 in Supporting information). In the iodine adsorption test, HCP-DAP, HCP-DETA and HCP-AA displayed the adsorption amount of 1708, 1253 and 1009 mg/g, respectively (Fig. 4d). As shown in Fig. 4e, the iodine adsorption processes of HCP-DAP, HCP-DETA and HCP-AA fitted well in pseudo-second-order kinetic model with high correlation coefficients (Table S6 in Supporting information) [52]. Like HCP-EDA, the characteristic peaks of C–C/C=C, C–N and N–H for HCP-DAP after iodine capture slightly shifted in C 1s and N 1s XPS spectra (Fig. 4b and Fig. S16 in Supporting information). The I 3d XPS spectra also proved the presence of both I_3^- and I_5^- in HCP-DAP/I (Fig. 4f). All these results revealed the superb generality of vapor-phase amination used various amines for improving iodine capture performances.

While the development of vapor-phase postsynthetic amination method in this study is highly encouraging, substantial challenges still need to be addressed in the future. First, a further understanding of the vapor-phase amination mechanisms is desired, since such insights will be indispensable in exploiting novel technology and large-scale production. Second, in contrast with the huge number of available porous materials, the number of samples that can be modified by vapor-phase amination is still limited. According to the good reactivity of amines toward halogen, acyl, hydroxyl and carboxyl groups, we envisage that, this vapor-phase amination strategy may be employed in postsynthetic functionalization of other porous materials (*e.g.*, MOFs and COFs) for various applications [28]. Third, the large-scale preparation conditions (*e.g.*, amination time and temperature) need to be further explored, which will provide an important guidance for the practical production of porous adsorbents in the iodine industry. Through the further efforts on these aspects mentioned above, we foresee a bright future for vapor-phase amination method.

In summary, we reported the vapor-phase postsynthetic amination of HCPs for enhancing their iodine capture performances. Through simple exposure in amine vapors, the halogen-containing HCP particles could be grafted by amines through nucleophilic substitution reaction. The introduced amino groups acted as electron-donor iodine-philicity binding sites to form strong charge-transfer interactions for the electron-deficient iodine molecules. In the iodine capture test, the amino-functionalized HCPs exhibited high iodine uptakes along with excellent reusability, about 221% adsorption capacity as that of original HCP-Cl. Mechanism analyses proved that the electron-donor N–H groups and π-conjugated benzene rings along with structure characteristics of high porosities, were critical factor for the iodine capture. Our vapor-phase amination strategy showed excellent generality and could be used by various amines. On the whole, the insights reported in this research may inspire the development of various vapor-

phase modification strategies for porous materials to extend their applications.

Declaration of competing interest

The authors declare that they have no known competing financial interests or personal relationships that could have appeared to influence the work reported in this paper.

Acknowledgments

This work was financially supported by National Natural Science Foundation of China (No. 22178143), Guangdong Basic and Applied Basic Research Foundation (Nos. 2021A1515110365 and 2020B1515120036), Natural Science Foundation of Anhui Higher Education Institutions (No. 2023AH050168), Innovation and Entrepreneurship Training Program for China College Students (No. 202310878049), Director Foundation of Anhui Province Engineering Laboratory of Advanced Building Materials (No. JZCL2305ZR) and Ph.D. Startup Foundation of Anhui Jianzhu University (No. 2023QDZ34).

Supplementary materials

Supplementary material associated with this article can be found, in the online version, at doi:10.1016/j.cclet.2023.109357.

References

[1] B. Zheng, X. Lin, X. Zhang, et al., Adv. Funct. Mater. 30 (2020) 1907006.
[2] Y. Xie, T. Pan, Q. Lei, et al., Nat. Commun. 13 (2022) 2878.
[3] W. Xie, D. Cui, S. Zhang, et al., Mater. Horiz. 6 (2019) 1571–1595.
[4] T. Pan, K. Yang, X. Dong, et al., J. Mater. Chem. A 11 (2023) 5460–5475.
[5] Y. Zhu, Y. Qi, X. Guo, et al., J. Mater. Chem. A 9 (2021) 16961–16966.
[6] M. Jia, S. Rong, P. Su, et al., Chem. Eng. J. 437 (2022) 135432.
[7] B. Li, R. Gong, W. Wang, et al., Macromolecules 44 (2011) 2410–2414.
[8] L. Tan, B. Tan, Chem. Soc. Rev. 46 (2017) 3322–3356.
[9] X. Li, G. Chen, H. Xu, et al., Sep. Purif. Technol. 228 (2019) 115739.
[10] G. Chen, Q. Zhao, Z. Wang, et al., J. Hazard. Mater. 434 (2022) 128859.
[11] A. Hassan, S. Goswami, A. Alam, et al., Sep. Purif. Technol. 257 (2021) 117923.
[12] X. Li, Z. Jia, J. Zhang, et al., Chem. Mater. 34 (2022) 11062–11071.
[13] X. Yan, Y. Yang, G. Li, et al., Chin. Chem. Lett. 34 (2023) 107201.
[14] Z. Yan, Y. Yuan, Y. Tian, et al., Angew. Chem. Int. Ed. 54 (2015) 12733–12737.
[15] D. He, L. Jiang, K. Yuan, et al., Chem. Eng. J. 446 (2022) 137119.
[16] X. Qian, B. Wang, Z. Zhu, et al., J. Hazard. Mater. 338 (2017) 224–232.
[17] Y.H. Abdelmoaty, T.D. Tessema, F.A. Choudhury, et al., ACS Appl. Mater. Interfaces 10 (2018) 16049–16058.
[18] X. Hu, H. Wang, C.F.J. Faul, et al., Chem. Eng. J. 382 (2020) 122998.
[19] H. Wang, N. Qiu, X. Kong, et al., ACS Appl. Mater. Interfaces 15 (2023) 14846–14853.
[20] C. Wang, Y. Wang, R. Ge, et al., Chem. Eur. J. 24 (2018) 585–589.
[21] S. Wang, Q. Hu, Y. Liu, et al., J. Hazard. Mater. 387 (2020) 121949.
[22] S. Xiong, J. Tao, Y. Wang, et al., Chem. Commun. 54 (2018) 8450–8453.
[23] X. Guo, Y. Li, M. Zhang, et al., Angew. Chem. Int. Ed. 59 (2020) 22697–22705.
[24] P. Su, X. Zhang, Z. Xu, et al., New J. Chem. 43 (2019) 17267–17274.
[25] C. Liu, Y. Jin, Z. Yu, et al., J. Am. Chem. Soc. 144 (2022) 12390–12399.
[26] S. Zhang, X. Tang, Y. Yan, et al., ACS Macro Lett. 10 (2021) 1590–1596.
[27] J.A. Martín Illán, S. Royuela, M.Mar Ramos, et al., Chem. Eur. J. 26 (2020) 6495–6498.
[28] Y. Yusran, X. Guan, H. Li, et al., Natl. Sci. Rev. 7 (2020) 170–190.
[29] V.A. Kuehl, P.H.H. Duong, D. Sadrieva, et al., ACS Appl. Mater. Interfaces 13 (2021) 37494–37499.
[30] Y. Xie, T. Pan, Q. Lei, et al., Angew. Chem. Int. Ed. 60 (2021) 22432–22440.
[31] S.J. Lyle, T.M. Osborn Popp, P.J. Waller, et al., J. Am. Chem. Soc. 141 (2019) 11253–11258.
[32] J.S.M. Lee, T. Kurihara, S. Horike, Chem. Mater. 32 (2020) 7694–7702.
[33] Y. Yin, Y. Yang, G. Liu, et al., Chem. Eng. J. 441 (2022) 135996.
[34] W. Xu, M. Niu, X. Yang, et al., Chin. Chem. Lett. 32 (2021) 489–492.
[35] W. Li, Z. Yang, W. Yang, et al., AIChE J. 68 (2022) e17517.
[36] N.A. Khan, R. Zhang, X. Wang, et al., Nat. Commun. 13 (2022) 3169.
[37] V. Rubio Giménez, G. Arnauts, M. Wang, et al., J. Am. Chem. Soc. 145 (2023) 152–159.
[38] N.A. Khan, R. Zhang, H. Wu, et al., J. Am. Chem. Soc. 142 (2020) 13450–13458.
[39] P. Su, M. Tu, R. Ameloot, et al., Acc. Chem. Res. 55 (2022) 186–196.
[40] W. Wu, J. Su, M. Jia, et al., Sci. Adv. 6 (2020) eaax7270.
[41] S. Rong, S. Chen, P. Su, et al., Inorg. Chem. 60 (2021) 11745–11749.
[42] P. Su, H. Tang, M. Jia, et al., AIChE J. 68 (2022) e17576.
[43] M. Huang, L. Yang, X. Li, et al., Chem. Commun. 56 (2020) 1401–1404.
[44] R. Shen, X. Yan, Y. Guan, et al., Polym. Chem. 9 (2018) 4724–4732.
[45] X. Zhu, S.M. Mahurin, S.H. An, et al., Chem. Commun. 50 (2014) 7933–7936.
[46] R. Dawson, T. Ratvijitvech, M. Corker, et al., Polym. Chem. 3 (2012) 2034.
[47] Y. Gu, S.U. Son, T. Li, et al., Adv. Funct. Mater. 31 (2021) 2008265.
[48] X. Li, G. Chen, J. Ma, et al., Sep. Purif. Technol. 210 (2019) 995–1000.
[49] A. Hassan, A. Alam, M. Ansari, et al., Chem. Eng. J. 427 (2022) 130950.
[50] D. Shen, T. Cai, X. Zhu, et al., Chin. Chem. Lett. 26 (2015) 1022–1025.
[51] Z. Shang, B. Zhao, Z. Wu, et al., ACS Appl. Mater. Interfaces 12 (2020) 56454–56461.
[52] X. Liu, A. Zhang, R. Ma, et al., Chin. Chem. Lett. 33 (2022) 3549–3555.
[53] B. Jiang, Y. Qi, X. Li, et al., Chin. Chem. Lett. 33 (2022) 3556–3560.
[54] J. Wang, K. Ai, L. Lu, J. Mater. Chem. A 7 (2019) 16850–16858.
[55] X. Li, Y. Peng, Q. Jia, Sep. Purif. Technol. 236 (2020) 116260.
[56] Z. Zhang, X. Dong, J. Yin, et al., J. Am. Chem. Soc. 144 (2022) 6821–6829.
[57] N. Mokhtari, M. Dinari, Sep. Purif. Technol. 301 (2022) 121948.
[58] N. Liu, H. Ma, R. Sun, et al., ACS Appl. Mater. Interfaces 15 (2023) 30402–30408.